Tidal asymmetry and velocity skew over tidal flats and shallow channels within a macrotidal river delta

N. J. Nidzieko[1,2] and D. K. Ralston[1]

Received 13 June 2011; revised 22 December 2011; accepted 27 December 2011; published 1 March 2012.

[1] It is often assumed that, in short, shallow estuaries, at leading order velocity and elevation are exactly out of phase, so that duration asymmetries in the rise and fall of the tide should be manifest as skewed velocities. We observed alternating ebb- and flood-dominant velocity skew in response to the spring-neap modulation of incident asymmetry generated by the mixed, mainly semidiurnal astronomical tides within the macrotidal Skagit River delta in Puget Sound, Washington. We describe three factors that may contribute to local asymmetries: (1) ebb dominance caused by phase lags between the surface gradient and local depth, (2) ebb dominance due to fluvial discharge, and (3) near-bed flood dominance due to baroclinicity. Large spring tides led to greater frictionally generated phase lags and resulted in ebb-dominant velocity skew. This ebb dominance caused by tidal drainage was reinforced by fluvial discharge across the tidal flat at lower-low water. The baroclinic component of this discharge, however, produced flood-dominant near-bed velocity skew that countered the ebb dominance of the frictional effects. The balance of these processes depends strongly on the spring-neap cycle, magnitude of river discharge, and position within the tidal flat and channel system. Our observations are notable in the context of previous studies describing these processes because our analyses indicate that these mechanisms are relevant over very short spatial scales of just a few kilometers and in very shallow systems.

Citation: Nidzieko, N. J., and D. K. Ralston (2012), Tidal asymmetry and velocity skew over tidal flats and shallow channels within a macrotidal river delta, *J. Geophys. Res.*, *117*, C03001, doi:10.1029/2011JC007384.

1. Motivation

[2] Two basic tidal asymmetries affect net sediment transport in most tidal embayments: peak velocity skew and slack water difference. The former is an Eulerian (local, time-varying) asymmetry that affects primarily bed load transport through different peak flood/ebb shear stresses [*Dronkers*, 1986; *Friedrichs and Aubrey*, 1988]; the latter is a Lagrangian (spatial) asymmetry that generally affects the finer suspended load through differential settling times and resuspension lags around high/low slack water [*Postma*, 1961; *Van Straaten and Kuenen*, 1958; *Pritchard*, 2005]. *Friedrichs* [2012] provides a thorough review of these processes as they pertain to tidal flats. Our effort here is to place our observations in the context of this theoretical framework.

[3] The tidal flats in this study are bisected by distributary channels that are part of a macrotidal river delta. This river discharge adds an additional level of complexity to examining asymmetric transport processes [e.g., *Scully and Friedrichs*, 2003; *Ralston and Stacey*, 2007], both through the imposition of a mean river flow and the resultant buoyancy forcing created within a shallow, energetic estuary. A fundamental understanding of the sources of tidal asymmetry is essential to placing these mechanisms in the broader context of wind-wave resuspension and episodic delivery of sediment via river discharge that collectively affect the long-term geomorphic evolution of coastal systems.

[4] In this paper we examine mechanisms that contribute to peak velocity skew within the tidal flats and distributary channels of the macrotidal Skagit River delta located in Skagit Bay, Washington (Figure 1a, inset). It is often assumed that, in short, shallow tidal embayments, at leading order velocity and elevation are exactly out of phase, so that duration asymmetries in the rise and fall of the tide should be manifest as skewed velocities. In Puget Sound, the tides are mixed, mainly semidiurnal and the interaction of the diurnal and semidiurnal astronomical constituents produces asymmetrical sea surface rise/fall durations that modulate on a fortnightly frequency with the change in diurnal inequality. We observed fortnightly variations in velocity skew within Skagit Bay that closely matched the incident duration asymmetry from Puget Sound, but with notable variations between neap and spring tides that indicate that cross-shore phase lags and baroclinicity are important, even in this short, shallow system. The motivation for this work is to examine how the incident asymmetry in the mixed astronomical tides contributes to

[1]Applied Ocean Physics and Engineering, Woods Hole Oceanographic Institution, Woods Hole, Massachusetts, USA.
[2]Horn Point Laboratory, University of Maryland Center for Environmental Science, Cambridge, Maryland, USA.

Copyright 2012 by the American Geophysical Union.
0148-0227/12/2011JC007384

velocity skew compared with transformations in velocity skew due to local frictional and baroclinic processes.

[5] In section 2 we provide a brief tidal asymmetry background, and define a method for quantifying duration asymmetry in the rise/fall of the sea surface and flood/ebb velocity skew. Section 3 describes the field observations. In section 4 we compare the observations to a rigid lid conceptual framework where flows are governed by continuity and bathymetry, and consider how deviations from this leading order approximation contribute to skewed velocities.

[6] There are three main mechanisms that we consider: (1) incident asymmetry from the tide, (2) ebb dominance that arises from system-wide phase lags relative to local changes in surface elevation, and (3) the role of river discharge in contributing ebb-directed velocity skew through mean discharge and flood dominance through baroclinic effects. These mechanisms are variable at event to fortnightly time scales, and highlight the need for both high-resolution and long-term observations in assessing estuarine dynamics.

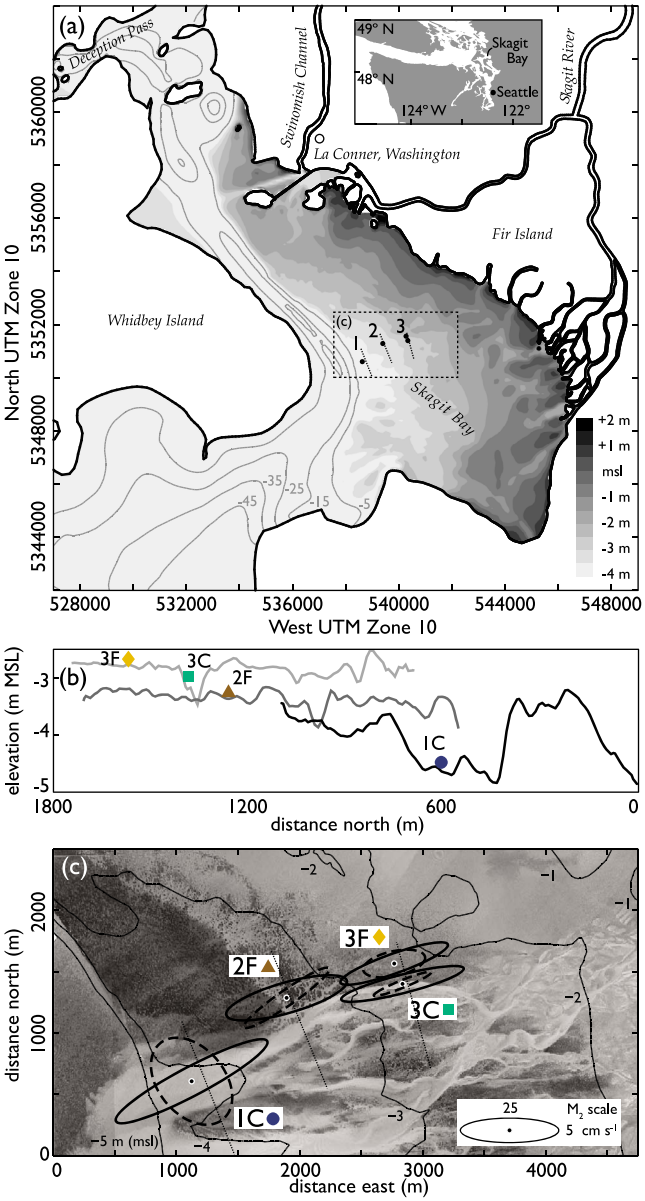

Figure 1. (a) Map and bathymetry of the Skagit Bay region. Elevation contours in the tidal flats region are labeled in meters relative to mean sea level, as indicated in shading scale. Contours below −4 m msl are unshaded and labeled accordingly. Station locations are denoted with solid circles, with numbers nominally denoting landward distance from the lip in km. Bathymetry profiles in Figure 1b are dotted lines; image in Figure 1c is outlined with dashed line. (b) Bathymetric profiles intersecting station locations. Profiles obtained as averaged bathymetry from boat-based observations on 3–5 June 2009. (c) Aerial image of study location. Stations located in a distributary channel are labeled with "C," while stations on adjacent flats are denoted with "F." M_2 velocity ellipses are shown in solid lines for each station, scaled according to the legend; M_4 velocity ellipses are shown in dashed lines, at 5 times the legend scale. The aerial image is from low water on 28 August 2000, 11:00 PDT. The water line can be seen below the −3 m contour; dark stippling below −2 m is benthic flora, predominantly eelgrass; and sediment-laden water in the distributary channel is lighter relative to the receiving water of Skagit Bay. Image copyright Skagit River System Cooperative, used with permission. Station colors and symbols are used here and in Figures 2, 4, and 7: 1C (blue circle), 2F (brown triangle), 3C (green square), and 3F (yellow diamond).

2. Background

2.1 Duration Asymmetry and Velocity Skew

[7] Tidal duration asymmetry (the difference in the duration and/or amplitude of rising and falling water) can arise from distortion of the tide in shallow water or from the interaction of astronomical tidal constituents. Tidal distortion generally increases with distance into a tidal embayment, and is manifest as the growth of overtides and higher harmonics created by nonlinear terms in the equations of continuity and momentum [*Heath*, 1980; *Parker*, 1991; *Friedrichs and Madsen*, 1992]. Physically, the crest of the tidal wave (high water) propagates faster than the trough (low water), so within the embayment there is a shorter period of rising water (from low water to high water) than falling water. High water propagation may be slowed if the intertidal volume of adjacent shoals is large relative to channel volume, resulting in a longer period of rising water [*Speer and Aubrey*, 1985; *Fortunato and Oliveira*, 2005].

[8] In embayments with predominantly semidiurnal tides, duration asymmetries due to distortion may be modeled as the superposition of the principal lunar semidiurnal M_2 and its first overtide, the lunar quarterdiurnal M_4. For mixed semidiurnal/diurnal tides, duration asymmetries arise from the interaction of astronomical diurnal constituents (K_1, O_1, and P_1) and semidiurnal constituents (M_2, S_2, and N_2) [*Hoitink et al.*, 2003]. Nonlinear distortion within the system either counteracts or reinforces this incident asymmetry [*Nidzieko*, 2010].

[9] Velocity skew is the asymmetrical distribution of ebb and flood tidal currents over a tidal cycle. This skew can be a local phenomenon caused by bathymetry, as in the case of

flows around a headland [*Geyer*, 1993], flows with curvature [*Nidzieko et al.*, 2009], or in channels with segregated flood/ebb conduits [*Ahnert*, 1960; *van Veen et al.*, 2005]. On a system-wide scale, shoaling bathymetry contributes to skewed velocities through the distortion of the surface tide, which results in differences between the duration of rising and falling water [*Boon and Byrne*, 1981], as described above. When velocity and water level phases are in quadrature, shorter-rising duration relative to falling requires faster flood velocities to convey the tidal prism in a shorter period; conversely, shorter-falling duration produces faster ebb currents.

[10] *Speer et al.* [1991] reported observations of shorter-rising duration asymmetry coincident with ebb-dominant discharges in tidal inlets along the U.S. East Coast. Similar observations were reported by *Lincoln and Fitzgerald* [1988], who termed the situation when the offshore tide is lower than the elevation of the estuarine bathymetry as truncation. *Speer et al.* [1991] described qualitatively that truncation lead to ebb dominance when the falling tide in the estuary decoupled from the offshore tide, such that the momentum balance within the estuary was essentially fluvial–where the barotropic pressure gradient defined by the bed slope was balanced by friction.

[11] Tidal flats necessarily truncate the tide by virtue of their intertidal position. Citing the work of *Speer and Aubrey* [1985] in tidal channels, *Dronkers* [1986] noted that the phase lag of ebb across a tidal flat relative to a deeper seaward channel would produce a sea surface slope that resulted in stronger ebb currents. *Friedrichs et al.* [1992] discussed this condition more rigorously, noting that an increased sea surface gradient on ebb occurred as the result of tidal stage dependence in friction-induced lags. The distributary channels bisecting the Skagit Bay tidal flats are not as deeply incised as those typically associated with an ebb-directed discharge [e.g., *French and Stoddart*, 1992], where a significant step change in velocity magnitude occurs above the elevation of the marsh. Our observations in Skagit Bay show evidence of enhanced ebb velocities due to late ebb sea surface setup; we will consider this ebb-directed enhancement in regard to the variable incident asymmetry and the flood-directed baroclinic contribution.

2.2. Quantifying Asymmetry

[12] Previous studies have utilized the presence and growth of overtides as a diagnostic tool for tidal asymmetry, as overtides (and other higher harmonics) can be indicative of nonlinear processes within a tidal estuary, embayment, or coastal sea [e.g., *Blanton et al.*, 2002; *Seim et al.*, 2006]. In systems dominated by the M_2 semidiurnal tide, the amplitude ratio a_{M_4}/a_{M_2} has been used to indicate the degree of nonlinearity, while the quadrant containing the phase difference $2\phi_{M_2} - \phi_{M_4}$ indicates the direction of asymmetry [*Friedrichs and Aubrey*, 1988].

[13] Because this method relies on harmonic analysis to extract tidal constituents from a time series, it is sensitive to record length. Neighboring constituent pairs, such as M_2 and N_2, cannot be resolved from records that are too short, and phenomena due to spring-neap cycles or weather band events are not resolved. Additionally, nonlinearities in velocity can be broad-banded and therefore not properly quantified with harmonic methods alone [cf. *Godin*, 1991]. We report observed harmonic amplitudes and phases in Appendix A for comparison against other records.

[14] Analysis of asymmetry is not feasible in Skagit Bay using amplitude ratios or phase differences, as the primary motivation in this study is to consider variations in asymmetry that change in less than a fortnight. A simple method of quantifying observed asymmetry is to calculate the third moment about zero, normalized by the second moment about zero to the 3/2 power:

$$\gamma_0 \equiv \frac{\mu_3}{\mu_2^{3/2}}, \tag{1a}$$

where the m-th moment about zero is defined as

$$\mu_m = \frac{1}{N-1}\sum_{i=1}^{N} (n_i)^m \tag{1b}$$

and N is the number of samples n_i. This is similar to skewness, which is typically defined as the normalized third moment about the mean (i.e., the third central moment [cf. *Emery and Thomson*, 2001]). In order to quantify tidal observations relevant to sediment transport, however, we use the third moment about zero, rather than about the mean. Sediment transport is roughly proportional to velocity cubed [*Bagnold*, 1966], so including the mean velocity in the skewness calculation provides a more relevant metric for sediment transport potential. For brevity, we will refer to the quantity in (1) as skewness, but emphasize that this is not identical to the skewness that might be calculated with a data analysis package such as MATLAB. *Nidzieko* [2010] showed that the M_4/M_2 -specific amplitude and phase relationships are contained in the more generic skewness calculation in (1), and demonstrated the utility of this metric in comparing water level observations in several U.S. west coast estuaries.

[15] Literature pertaining to surface gravity waves makes a distinction between the terms skewness and asymmetry–the former refers to the normalized third moment of velocity, and the latter to the normalized third moment of vertical water level accelerations (i.e., the time derivative of water level) [*Elgar and Guza*, 1985]. In tidal and sediment transport literature, the term asymmetrical has been used to refer both to rise/fall duration asymmetry and velocity skew. In this paper we use skewness as defined in (1) to quantify skew in across-shore tidal velocities γ_0^U by substituting $n = u$; duration asymmetry in the rise and fall of water level $\gamma_0^{\zeta_t}$ is quantified by substituting the time derivative $n = \zeta_t \equiv \partial\zeta/\partial t$. For velocity, the tide is ebb dominant for $\gamma_0^U < 0$ and flood dominant for $\gamma_0^U > 0$; the duration of falling water is shorter than rising water for $\gamma_0^{\zeta_t} < 0$ and longer for $\gamma_0^{\zeta_t} > 0$.

[16] If currents and elevation are exactly in quadrature, the skewness numbers (duration asymmetry and velocity skew) will be identical. Thus, differences between duration asymmetry and velocity skew

$$\Delta\gamma_0 = \gamma_0^U - \gamma_0^{\zeta_t} \tag{2}$$

can be diagnostic of how tides are manifest as currents on the tidal flat. Negative $\Delta\gamma_0$ indicates enhanced velocity ebb dominance (or less flood-dominant velocities depending on

Table 1. Deployment Locations in Skagit Bay

Station	Latitude, Longitude	z[a] (m msl)	x[b] (km)	$C_d \times 10^3$ [c]	$\frac{S_0}{B_0}$[d]	$\frac{B_0}{S_0}(6 \times 10^{-4})$[e]	R^2 [f]
1C	48° 18′ 26.9″N, 122° 28′ 44.9″W	−4.5	0.4	1.3	3.8×10^{-4}	1.6	0.95
2F	48° 18′ 28.8″N, 122° 28′ 7.2″W	−3.5	1.4	3.2	5.5×10^{-4}	1.1	0.95
3C	48° 18′ 52.3″N, 122° 27′ 21.4″W	−3.0	2.3	2.7	4.9×10^{-4}	1.2	0.90
3F	48° 19′ 3.7″N, 122° 27′ 25.2″W	−2.7	2.3	2.5	5.9×10^{-4}	1.0	0.93

[a]Here z is the elevation of the station relative to mean sea level.
[b]Here x is the distance from the seaward edge of the tidal flat at −5 m.
[c]C_d, which varied with stratification, is reported for $N = 0$.
[d]Assuming a rigid lid, linear regression between depth-averaged velocity and ζ_t (Figures 5a and 5b) indicates the ratio of bottom slope S_0 to average width factor B_0 is 4×10^{-4} to 6×10^{-4}.
[e]The bottom slope inferred from bathymetry data was 6×10^{-4}, which would yield mean width factors of 1 to 1.6, decreasing with distance up-flat.
[f]The R^2 statistic is for the linear regression between ζ_t and U for all observations at that station.

the signs of γ_0^U and γ_0^ζ) relative to the rise/fall asymmetry in the sea surface.

[17] Finally, in this paper asymmetry and skew are quantified by computing the third moment of observations with a running discrete lunar day (24.84 h) window advanced between times of lower-low water (LLW); the averaging period for 16 June is only 12.42 h to account for the minimal diurnal influence during the neap tide. The running third moment is normalized by the second moment (variance about zero) of the entire time series to the 3/2 power in order to preserve magnitude information between spring-neap tides, such that normalized values are not confined to the range $\{-1, 1\}$. Using times of LLW prevents aliasing fortnightly variations in tidal range into the time average.

3. Skagit River Delta and Tidal Flats System

[18] Skagit Bay is part of the Salish Sea, located east of Whidby Island between Saratoga Passage to the south and Deception Pass to the north. The sandy tidal flats bordering the northeast shoreline of Skagit Bay are delta topset formed by fluvial discharge from the Skagit River, which splits into north and south forks 3 miles south of Mount Vernon, Washington. The historic delta was levied for agricultural purposes, creating Fir Island and producing tidal flats that are bordered to the north and south by braided distributary channels from the two forks. At high water, Skagit River discharge spreads broadly across the intertidal region, creating a shallow estuary. At lower-low water (LLW), most of the flats are exposed and freshwater discharges across the flat are confined to shallow, distributary channels with typical depths of 0.5 to 1 m [*Ralston et al.*, 2012]. We will refer to the subtidal and intertidal areas of this delta topset feature collectively as Skagit Bay for succinctness.

[19] The main region of Skagit Bay (Figure 1a) extends 15 km in the alongshore direction (with respect to a coordinate aligned with isobaths) and 3–6 km in the across-shore direction. The tidal range is 3–5 m; diurnal and semidiurnal tidal constituents have similar amplitudes a, with a form factor $F = (a_{K_1} + a_{O_1})/(a_{M_2} + a_{S_2}) = 1.15$. The offshore lip of the delta topset is approximately 5 m below mean sea level (msl), and borders a 2 km wide channel of O(30 m) depth. Eelgrass is the dominant vegetative cover in the lower tidal flats; the upper elevations of the flats are bordered by marsh vegetation near mean higher-high water (MHHW). The delta topset sediments within Skagit Bay are primarily sands (>75% of surface area consists of 0.6–4 mm diameter grain size [*McBride et al.*, 2006]). And there is evidence of regular reworking of the upper tens of cm of sediments as distributary channels migrate (K. L. Webster et al., Delivery, reworking and export of fine-grained sediment across the sandy Skagit River tidal flats, Washington State, submitted to *Continental Shelf Research*, 2011).

[20] Average discharge for the period of record on the Skagit River at Concrete, WA (water years 1925–2008 at USGS station 12194000) was 425 $m^3 s^{-1}$. The Skagit River splits into north and south forks 3 miles south of Mount Vernon, Washington (river mile 12), with 35%–45% of the discharge conveyed via the south fork (C. Curran et al., Sediment load and distribution in the lower Skagit River, Washington, USA, submitted to *Continental Shelf Research*, 2011).

3.1. Data Collection

[21] We deployed instrumented platforms in Skagit Bay (Figure 1 and Table 1) from 2 June to 28 June 2009. Water velocity and hydrographic parameters were measured at an array of across-shore stations: three sets of stations (nominally 1, 2, and 3 km from the lip) were located along the northernmost south fork distributary channel. Stations located in the distributary channel are denoted with "C"; those on the adjacent flats, north of the channel, are denoted with "F." Each station comprised a bottom-mounted, upward looking acoustic Doppler current profiler, conductivity-temperature-pressure recorders on a bottom-mounted frame and a surface float, and an acoustic Doppler velocimeter (ADV) with the sample cell nominally 45 cm above the bed. The current profiler at 1C was deployed for a longer period, from 2 June to 27 July 2009. All observations were averaged into 10 min intervals. Depth-averaged and near-bed (lowest profiler bin) velocities were linearly interpolated across low-slack water when the water depth was too shallow for the bottom-mounted acoustic profiler to operate.

[22] Bed stress estimates (u_*^2) were made by fitting an inertial subrange to ADV burst data [*Huntley*, 1988]. The ADV-derived stress measurements were noisy and incomplete at times when the water was shallow, which affected our ability to calculate a drag coefficient. A smoothed, continuous estimate of the drag coefficient, $C_d = u_*^2/u^2$, was obtained by fitting a curve of C_d as a function of buoyancy frequency at each station, to account for changes in the bed stress due to stratification (not shown). The effective C_d at $N = 0$ is listed in Table 1. Water level observations were

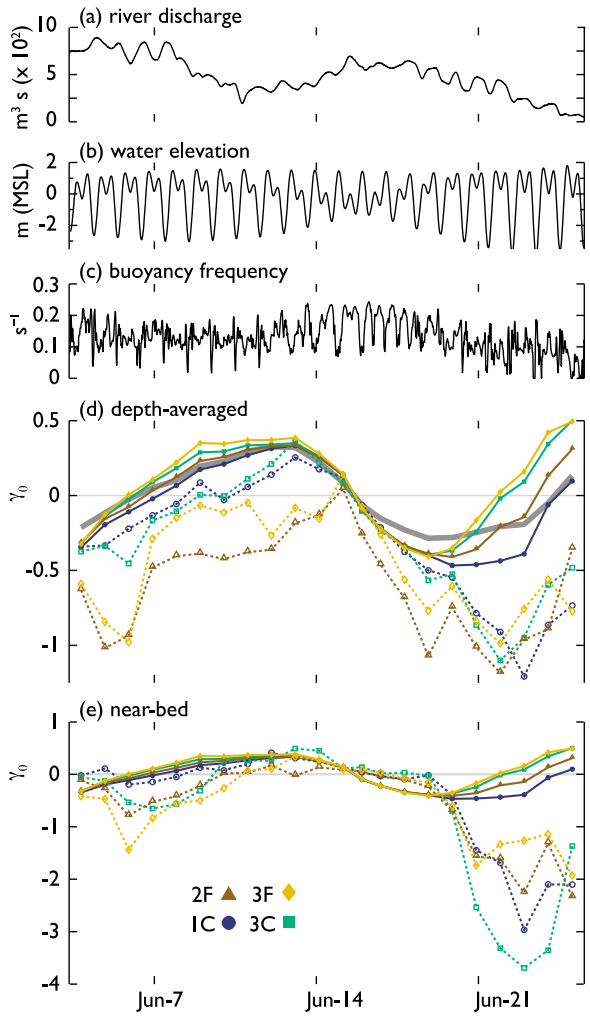

Figure 2. (a) Discharge at Mount Vernon (gray line). Average discharge for the period of record on the Skagit River at Concrete, Washington (water years 1925–2008 at USGS station 12194000), was 425 $m^3\ s^{-1}$. (b) Water level at 1C. (c) Buoyancy frequency N at 1C. (d) Tidal duration asymmetry (solid lines, filled symbols) and depth-averaged velocity skew (dashed lines, open symbols). Duration asymmetry and velocity skew, measured with equation (1a), co-oscillate with the incident asymmetry from Puget Sound, as recorded at Seattle (thick gray line in Figure 2d). (e) Duration asymmetry, as in Figure 2d, and near-bed velocity skew (dashed lines, open symbols). Station symbols are listed and are the same as in Figure 1.

adjusted to a common vertical datum by assuming a flat sea surface at high tide during the neap tides on 15–17 June.

[23] Skagit River discharge data was obtained from USGS stations 12194000 (near Concrete, WA) and 12200500 (near Mount Vernon, Washington). Observations of water level in Puget Sound were obtained from National Ocean Service Seattle tide gauge 9447130.

3.2. Observations

3.2.1. Hydrography and Velocities

[24] Observed river discharge and hydrographic conditions are shown in Figures 2a–2c. Hourly river discharge peaked around 900 $m^3\ s^{-1}$ on 6 June and 15 June and had diurnal variations of 100 $m^3\ s^{-1}$ due to power generation upstream. Stratification was strongest and most persistent at the start of the experiment when discharge was highest, and during neap tides from 14–20 June. Tidal straining produced a midebb stratification maximum, followed by well-mixed conditions late ebb and during most of the flood.

[25] Tidal currents were strongest in the across-shore direction. Peak velocity magnitudes were 0.5 to 1.0 m s^{-1}; along-flat velocities were O(0.25 m s^{-1}). Velocity magnitude decreased with distance landward and between adjacent stations on the channel and flats, evident in both the velocity examples in Figure 3 and the harmonic ellipse parameters in Table A2. The results of the harmonic analyses for both elevation and velocity are contained in Appendix A, Tables A1 and A2, respectively.

[26] Three tidal cycles are shown in Figure 3, representative of changes in greater diurnal range and diurnal inequality with the progression through the spring-neap cycle (Figure 2b). These examples highlight both the changing incident asymmetry through the spring-neap cycle and the cross-shore phase lags between stations.

[27] The mixed semidiurnal tides can have large diurnal inequalities where HHW follows LLW (Figure 3a) or HHW precedes LLW (Figure 3b). Spring tides can have double tides with nearly equal high water (Figure 3c). Because of these large diurnal inequalities, we found that the most representative depth for a diurnal tidal cycle was mean tide depth $\bar{H} = \frac{1}{2}(H_{\mathrm{HHW}} + H_{\mathrm{LLW}})$, rather than mean depth, as the depth of the water column during the small ebb and small flood are irrelevant to dynamics around LLW.

[28] For most of the observations, water level changes at Seattle and in Skagit Bay are similar; amplitudes and phases of the principal astronomic constituents for the two locations are nearly identical (Table A1) and so we use the Seattle gauge as a reference location unaffected by the frictional effects in Skagit Bay. Water levels on the tidal flat (i.e., 2F and 3F) and in the distributary channel (1C and 3C) were nearly indistinguishable with the exception of during the lowest tides (Figure 3c). In addition to these intrastation differences at extreme low water, there were systematic differences between Seattle and in Skagit Bay during spring tides (Figures 3a and 3c). On flood, the timing of peak ζ_t on the flat lagged Seattle by up to 1 h, with peak velocities occurring at or after peak ζ_t. These large floods were well mixed, with $\mathrm{Ri}_b \equiv N^2/S^2 < 1$, where N is the bulk buoyancy frequency and S is the top-to-bottom velocity shear. The cross-shore divergence of ζ_t is also evident during these large spring tides (see 1C and 3C at the start of flood in Figure 3c).

[29] During the small ebb and small flood, as well as during neap tides, ζ_t in Skagit Bay and at Seattle were nearly indistinguishable. Inertial effects were evident for these smaller vertical excursions and velocity lagged ζ_t by up to 15 min, presumably due to persistent stratification throughout these periods.

[30] On the large ebb, ζ_t initially lagged Seattle by 10–20 min, and was nearly constant across Skagit Bay when Ri_b was greater than 1. When Ri_b decreased below 1, the momentum balance was primarily between barotropic pressure gradient and bottom friction. This is most evident in the

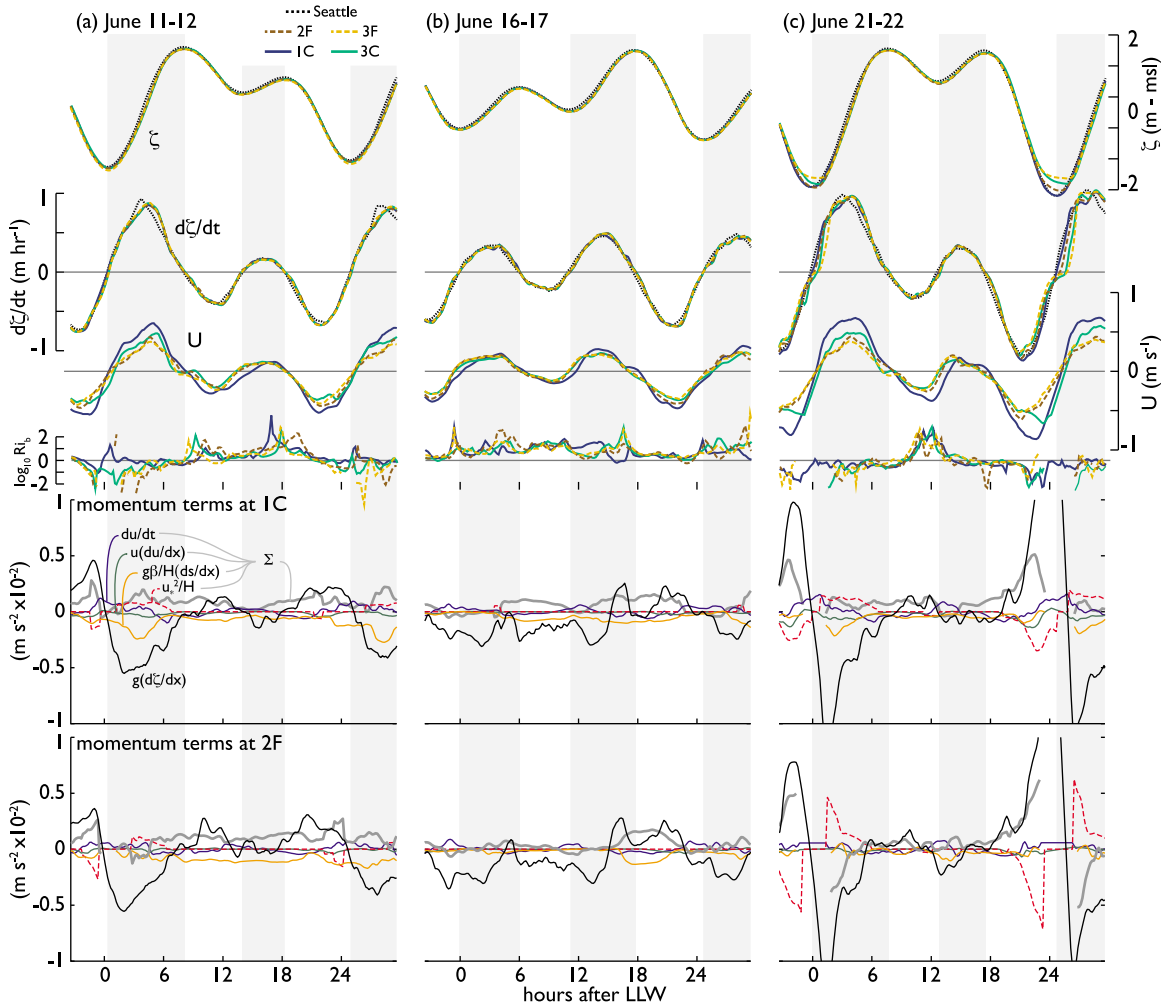

Figure 3. Representative mixed, mainly semidiurnal tidal cycles from Skagit Bay with different greater diurnal range and diurnal inequality. From top to bottom, traces are sea surface height, ζ_t, depth-averaged across-shore velocity, and Ri_b. Channel locations are shown with solid lines, and flats are shown with dashed lines. Seattle observations are shown with dotted lines. Gaps in Ri_b for Figure 3c are undefined when top and bottom current profiler bins are the same. Figures 3a (bottom), 3b (bottom), and 3c (bottom) show momentum terms for 1C calculated as finite differences between 1C and 3C and for 2F calculated as finite differences between 2F and 3F. (a) Typical spring tides when higher-high water (HHW) follows lower-low water (LLW). (b) Neap tides where HHW precedes LLW. (c) Perigean spring tides during the solstices. The double high tides are of near-equal elevation, although the duration of rising water is shorter.

example from 21–22 June. Maximum velocities on the flat (2F and 3F) were nearly coincident with peak ζ_t on ebb; maximum velocities in the channel (1C and 3C) occurred up to 3 h later.

[31] Momentum budget terms were calculated as a finite difference approximation between 1C and 3C, and between 2F and 3F, shown in Figures 3a (bottom), 3b (bottom), and 3c (bottom). The strength of the baroclinic pressure gradient decreased between 11 June and 21 June with reduced discharge, and the magnitude of the barotropic pressure gradient increased with larger tidal range. Each of these terms was similar on the tidal flat and in the distributary channel. The sum of all terms excluding the barotropic pressure gradient was similar to the measured barotropic pressure gradient; this sum was the same order of magnitude for most of the tidal cycle, but typically underestimated the barotropic pressure gradient on ebb by a factor of 2 and frequently missed the large flood component completely, highlighting the complexities of flows in this region.

3.2.2. Tidal Asymmetry

[32] The tide within Skagit Bay alternated between positive and negative duration asymmetry, as measured with (1), on a roughly fortnightly period (Figures 2d and 2e). The tides during the transition from neap to spring were negative asymmetric, while tides during the spring to neap transition were positive asymmetric. The variable asymmetry followed the incident asymmetry from Puget Sound (gray line in Figure 2d), only deviating significantly during the larger perigean spring tides (20–24 June).

[33] Velocities were affected by the incident duration asymmetry and alternated fortnightly between ebb dominant (negatively skewed) and flood dominant (positively skewed).

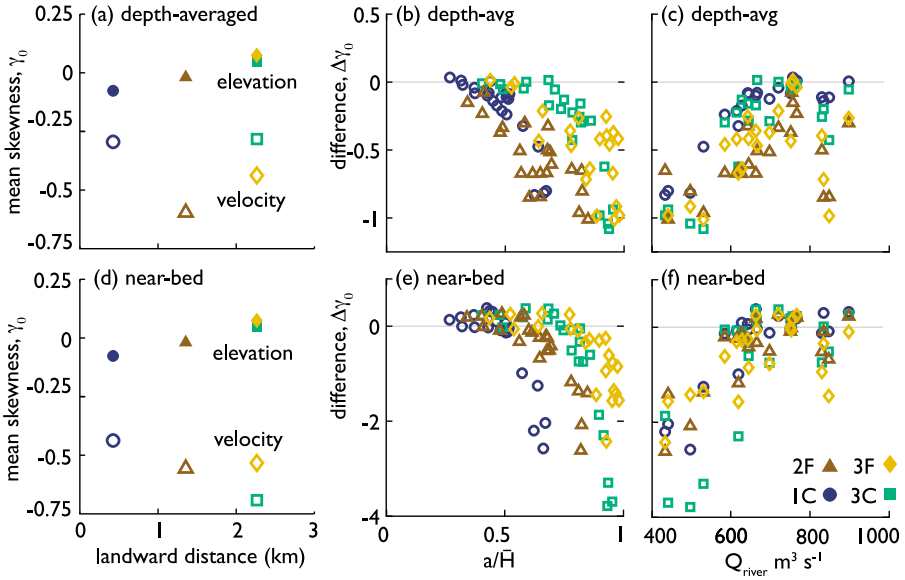

Figure 4. Skewness as a function of distance across shore, tidal amplitude-to-depth ratio $a/\bar{H}$, and daily mean river discharge Q_r. Figures 4a–4c are for depth-averaged velocity, and Figures 4d–4f are for near-bed velocity. Figures 4a and 4d include the average skewness for the entire record for surface elevation (close symbols) and velocity (open symbols). Figures 4b, 4c, 4e, and 4f show the difference between duration asymmetry and velocity skew, $\Delta\gamma_0$. Ebb dominance increases for larger tides (Figures 4c and 4e), while near-bed flood dominance increases as function of discharge. Station symbols are shown in Figure 4b and are the same as listed in Figure 1.

Depth-averaged velocity skew was always less than duration asymmetry (Figure 2d), whereas near-bed skew was observed to be flood dominant during neap tides, even when duration asymmetry and depth-averaged velocity skew were negative (Figure 2e). Velocities were most negatively skewed during the perigean spring tides despite positive duration asymmetry.

[34] Spatially, these observations can be summarized as follows. The tidal elevations were increasingly positive asymmetric with landward distance (Figure 4a), consistent with predictions for the growth of flood-dominant overtides in a shallow tidal estuary [*Speer and Aubrey*, 1985; *Friedrichs and Aubrey*, 1988]. Velocity skew decreased landward between stations 1C and 3C, and between 2F and 3F, though all observations were ebb dominant relative to duration asymmetry. Depth-averaged velocities on the flats tended to be more negatively skewed than in the channel (Figure 4a). Near-bed velocity skew became more negative with landward distance, but was less negatively skewed on the flat at 3F than in the channel at 3C (Figure 4d). This temporal averaging over the observational period is somewhat arbitrary, however, as the observations include an incomplete spring-neap cycle (i.e., we observed two spring periods and only a single neap period); with a longer record the relative spatial pattern would remain similar though the absolute numbers would change. In general, the temporal variance caused by the incident asymmetry through the spring-neap cycle was equal to or greater than the spatial variance between stations. The mean incident duration asymmetry was near zero, however, and so the change in asymmetry and skew with distance landward points to additional mechanisms as important sources of skewness.

[35] In Figures 4b and 4e, differences $\Delta\gamma_0 = \gamma_0^U - \gamma_0^\zeta$ are shown as a function of $a/\bar{H}$ for depth-averaged velocity and near-bed velocity, respectively. Depth-averaged velocity skew was more ebb dominant as a function of increasing tidal range, while near-bed velocity skew was more flood dominant for neap tides and larger discharges. In Puget Sound there is greater variance in the elevation of LLW than HHW through the spring-neap cycle (Figure 2b; see also Figure 13a), such that spring tides have much lower LLW elevation than neap tides and the effective depth around LLW is shallower; consequently $a/\bar{H}$ increases nonlinearly with the spring tides. $\Delta\gamma_0$ is also shown in Figures 4c and 4f as a function of changing river discharge. Although shifts in tidal forcing appeared to be more significant than changes in discharge at altering $\Delta\gamma_0$, some of the enhanced ebb-dominant skew at lower discharges occurs because the lower tidal water levels during the perigean spring tide increase the area of the tidal flat/delta that has channelized river discharge.

4. Sources of Asymmetry

[36] The observations can be summarized in three general points. One, skewed velocities are partly due to duration asymmetries imposed externally from Puget Sound. This incident asymmetry modulates fortnightly with the phasing of the principal diurnal and semidiurnal astronomic constituents. Two, nonlinear distortion with increasing landward distance results in positive duration asymmetry, though velocities remained negatively skewed. Three, the river discharge has a baroclinic effect as near-bed velocity skew can be flood dominant even when duration asymmetry is negative; this baroclinic effect offsets the ebb-directed transport associated with a mean river flow. These three conditions

are discussed in an analytic framework in this section. In section 4.1 we clarify how asymmetry in the incident tide will contribute to velocity skew. In section 4.2 we describe how frictionally generated phase lags lead to ebb dominance. In section 4.3 we show how tidally variable stratification can lead to near-bed flood dominance and contrast this against the ebb-directed fluvial discharge.

4.1. Asymmetry in the Incident Tide

[37] A common simplification in short, shallow tidal embayments is to assume that phase lags across the estuary are negligible, such that water level essentially rises and falls uniformly like a rigid lid [*Friedrichs and Aubrey*, 1996; *Pritchard and Hogg*, 2003; *Fagherazzi et al.*, 2003]. In this limit, velocity and elevation are exactly out of phase with one another (in quadrature) and so duration asymmetries are manifest as skewed velocities.

[38] The quadrature phase relationship between velocity and elevation in a short system with no river inflow can be found by starting from a width- and depth-integrated continuity equation

$$b\zeta_t = -(bHU)_x, \tag{3}$$

where $\zeta(x, t)$, $H(x, t)$, $b(x)$, and $U(x, t)$ are sea surface elevation, local depth, local width, and the depth- and width-averaged velocity, respectively. The time coordinate is t and x is the along-flow coordinate, zero at the seaward boundary and positive landward. Subscript t and x indicate partial differentiation. The local depth is defined as $H(x, t) = \zeta(x, t) - z(x)$, where $z(x)$ is the elevation of the bed relative to the same datum as the sea surface.

[39] Linearizing tidal elevation $\zeta = \zeta_0 + \zeta'$ where $\zeta_{0,x} \equiv 0$ and $\zeta' \equiv x\zeta_x$, and integrating from some position x landward to the position of the tidally variable shoreline $x_f(t)$, where the depth $H(x_f) \equiv 0$, (3) may be expanded

$$\zeta_{0,t}\int_x^{x_f} b\,dx + \int_x^{x_f} b\zeta_t'\,dx = bHU|_x. \tag{4}$$

[40] Neglecting the sea surface slope (second term in (4)), velocity at x is constrained by the local bathymetry and the rate at which the intertidal portion of the embayment landward of x fills and drains:

$$U_0(x,t) \equiv \zeta_{0,t}\frac{(x_f - x)}{H}B. \tag{5}$$

The subscript zero indicates the linearized solution. The width function

$$B(x_f \geq x) \equiv \frac{1}{2}\left(\frac{b(x_f)}{b(x)} + 1\right)$$
$$B = 0, \text{otherwise}$$

accounts for changing surface area as a function the position of the shoreline in an embayed ($b_L > b_0$) or lobate ($b_L < b_0$) coast [*Friedrichs and Aubrey*, 1996], where b_0 and b_L are the width of the flat at the seaward and landward boundaries, respectively. For a tidal flat with a linear width increase with distance across shore, $b(x) = b_0 + (b_L - b_0)\frac{x}{L}$. In the southern portion of Skagit Bay, the geometry of the embayment suggests $b_L \approx 3b_0$ and so B should vary between 1 and 2 as a function of tidal elevation and horizontal position. (See *Prandle and Rahman* [1980] for a discussion of embayment geometry on tidal flows.)

[41] When the sea surface gradient is neglected, the term $\frac{x_f - x}{H}$ in (5) provides a finite difference approximation to the bed slope S_0: $\frac{x_f - x}{\zeta_0 + z(x)} = \frac{x_f - x}{z(x_f) - z(x)} = \frac{1}{S_0}$. Provided that the longitudinal cross-sectional area is weakly convergent [*Friedrichs and Aubrey*, 1994], the linearized solution only depends on ζ_0 through B:

$$U_0 = \zeta_{0,t}\frac{B_0}{S_0} \tag{6}$$

With $B_0 \equiv B(\zeta_0)$ positive and exactly out of phase with $\zeta_{0,t}$ (as required for the linear solution), embayment geometry can only contribute to the magnitude and timing of peak velocity symmetrically about slack water, not to the directionality. Any duration asymmetry, whether incident or internally generated, will translate to velocity skew directly through $\zeta_{0,t}$ and velocity and elevation should be exactly out of phase. Equation (6) provides the rationale for comparing velocity skew and duration asymmetry with (1).

[42] The correspondence between observed U and ζ_t was predominantly linear (Figures 5a and 5b), with linear regression accounting for >90% of the variance and S_0/B_0 in the range 4×10^{-4} to 6×10^{-4} (Table 1). Equation (6) therefore provides a good leading order explanation for the observed spring-neap variations in velocity skew as a function of incident asymmetry in ζ_t. The largest departure from this linear relationship was below midtide at station 1C (not shown). This deviation was greater for locations in the distributary channel (compare 3C and 3F in Figures 5a and 5b) as the fluvial discharge contributed more to velocities in the channel.

[43] Equation (5) can be rearranged into a quadratic equation to evaluate x_f from observations. The mean position of $x_f(\zeta)$, shown as a solid line in Figures 5c and 5d, is a reasonable estimate of the bathymetric profile; the regressed slope is close to the mean bed slope inferred from bathymetric data ($S_0 = 6 \times 10^{-4}$) and the convex shape is consistent with an equilibrium profile for an embayed shoreline and the dominance of tidal energy relative to wave energy [*Friedrichs and Aubrey*, 1996; *Kirby*, 2000]. The mean position of x_f inferred from 3C is affected by discharge from the river, such that the apparent position of the shoreline is farther landward relative to 3F (broken line in Figure 5c).

[44] The depth-dependent deviation from a linear relationship between U and ζ_t appears as a systematic flood/ebb deviation in x_f. On flood, x_f was seaward of x_f on ebb for any given elevation below midtide, indicating a lag in the position of x_f relative to where a flat sea surface would intersect the shore. The sketch in Figure 6 shows how a lagged shoreline position requires a sea surface gradient. The scale of this lagged shoreline position inferred from Figures 5c and 5d is O(1000 m), which translates to a vertical elevation difference of 0.6 m for a linear slope of $S_0 = 6 \times 10^{-4}$. Using this elevation difference, an estimate of the barotropic pressure gradient across the lower flat (2.3 km from the offshore boundary) below midtide is $g\frac{\Delta\zeta}{\Delta x} \approx (10\ \text{m s}^{-2})\frac{(0.6\,\text{m})}{(2300\,\text{m})} \approx$

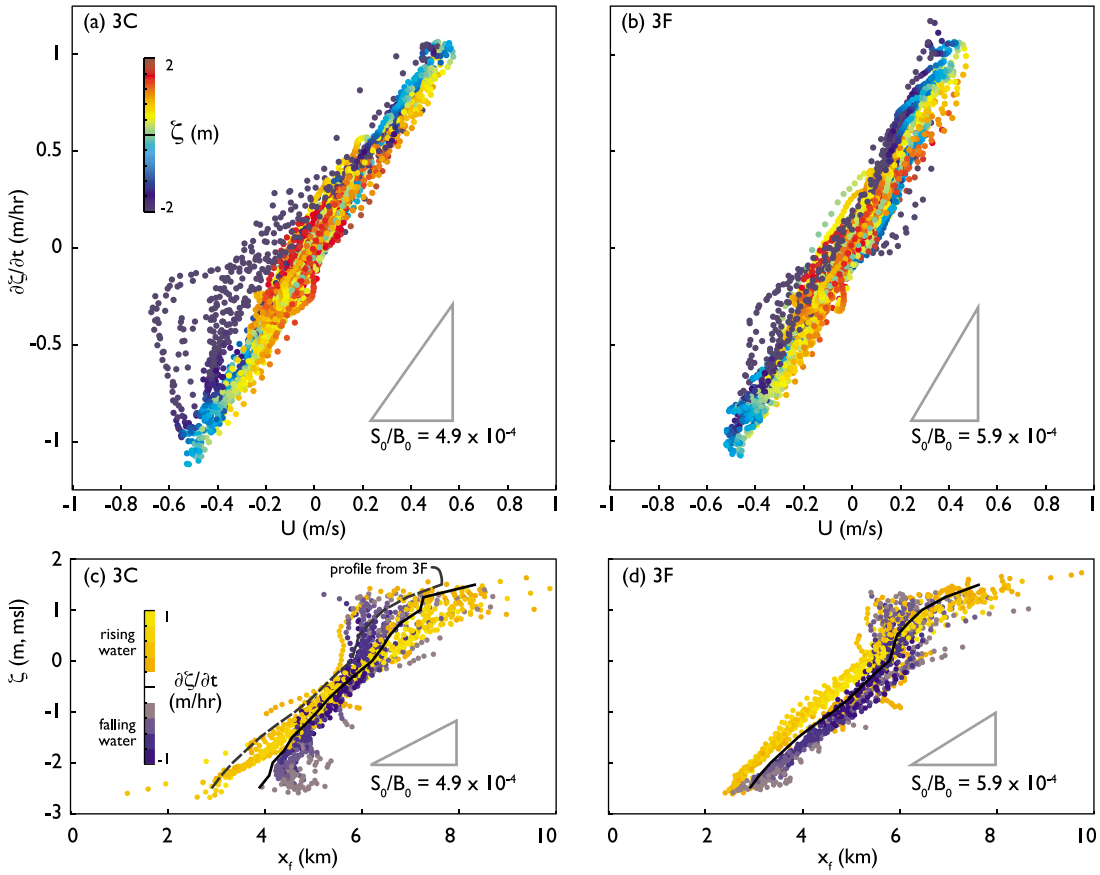

Figure 5. (a and b) Regression between observed depth-averaged velocity U and ζ_t at 1C and 3C provides a linearized estimate of bottom slope. Color shading indicates elevation of observations. (c and d) The position of the wetted front x_f inferred from observations and assuming a rigid lid. Color shading indicates rising or falling water. Only observations for $\bar{U} > 0.2$ m s^{-1} and $\bar{\zeta}_t > 0.2$ m h^{-1} are shown. The regressed bottom slopes from Figures 5a and 5b are shown.

3×10^{-3} m s^{-2}, consistent with the momentum terms in Figures 3a and 3c. Based on these observations we conclude that, although a rigid lid approximation provides a good leading order estimate for velocity, the sea surface gradient cannot be neglected when considering the higher-order velocity skew in our observations.

4.2. Enhancement of Ebb-Dominant Velocities via Surface Pressure Gradient Phasing

[45] In order to neglect the surface gradient in (4) and reach a linearized solution (equation (6)), we required $\zeta' \ll \zeta_0$. Defining the relevant horizontal and vertical length scales to be the tidal range and cross-shore distance of the tidal flats, respectively, $\zeta_0 \sim 2a$ and $\zeta' \sim L\zeta_x$ and so the maximum sea surface setup across the tidal flats must be small compared to the tidal range:

$$L\zeta_x \ll 2a. \tag{7}$$

This constraint is the same as the requirement of *Friedrichs* [2010] for a "short" estuary. If ζ_x and a are independent of one another, a rigid lid approximation should be more applicable for larger tidal ranges and hence more applicable at spring tide than at neap tide. In contrast, we observed increased ebb dominance as a function of $a/\bar{H}$ (Figures 4b and 4e).

[46] For spring tides if we assume a steady state momentum balance between barotropic pressure gradient and friction (Figures 3a and 3c), the surface slope scales as

$$\zeta_x \approx \frac{C_d U^2}{g\bar{H}}. \tag{8}$$

Combined with a velocity scale from continuity (equation (6))

$$U \approx a\omega \frac{B_0}{S_0}, \tag{9}$$

the requirement for a rigid lid (equation (7)) becomes

$$\frac{L}{2a}\zeta_x \approx \frac{1}{4}\frac{C_d}{g\bar{H}}\frac{a\omega^2 B_0^2 L}{S_0^2} = (kL)^2 \ll 1, \tag{10}$$

where

$$k^2 = \frac{1}{4}\frac{C_d}{g\bar{H}}\frac{a\omega^2 B_0^2}{S_0^2 L} \tag{11}$$

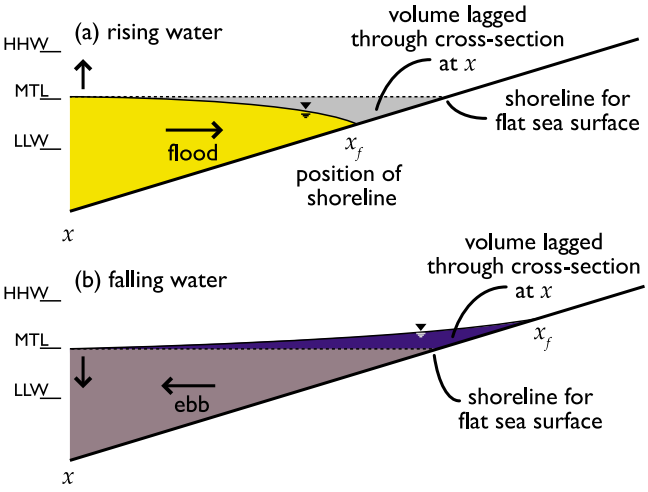

Figure 6. Sketches of lag between position of the tidally variable shoreline x_f and the position where a flat sea surface would intersect the bathymetry, for (a) rising and (b) falling water. The solid thin line depicts the sea surface, and the dotted line depicts a flat sea surface based on the tidal elevation at x. The gray-shaded area on flood is the volume deficit as compared to a rigid lid approximation. The dark blue is the lagged volume on ebb.

The term kL is evaluated in Figure 7 against differences between asymmetry and skew. Both depth-averaged and near-bed velocity skew were more negative than tidal duration asymmetry for increasing kL. This implies that the applicability of a rigid lid in Skagit Bay decreases during spring tides because a, H, and C_d all covary from neap to spring tides as friction becomes important relative to inertia: amplitude increases, mean tide depth decreases, and stratification is mixed out (Figures 2b and 2c). Based on our observations, velocity skew was ebb dominant relative to duration asymmetry for $kL > 0.1$, regardless of baroclinicity and location within the lower intertidal portion of the system that we observed (Figure 7).

[47] We have written the requirements for a short estuary approximation using notation k because the dependencies in (10), which we derived through scaling arguments, are functionally the same as those of the complex wave number k found in the solution to a diffusive wave equation, where the diffusion constant D is related to the wave number as $k_0^2 = \frac{i\omega}{2D}$ [*Friedrichs and Madsen*, 1992]. Increasing kL, or equivalently decreasing tidal diffusion, means a greater phase lag and consequently a larger surface setup, as evidenced by the setup inferred from a lagged x_f (Figures 5c and 5d).

[48] At the tidal time scale, *Friedrichs and Madsen* [1992] showed that the surface gradient provides a feedback of energy to the principal tidal harmonic for diffusive tide propagation. Time-varying diffusion is slowest when the surface gradient, and therefore velocity, is largest [*LeBlond*, 1978]. In the context of our observations over the spring-neap cycle, this is consistent with larger kL (Figure 7) leading to stronger ebb velocities relative to a given tidal duration asymmetry (Figure 2). This same mechanism produces ebb-dominant velocities at inlets, despite a longer falling tide and flood-dominant interior marshes [*Speer et al.*, 1991; *Friedrichs et al.*, 1992].

[49] The consequence of a lagged surface gradient relative to local depth is that the difference between velocity skew and duration asymmetry will always be negative. This is illustrated in Figure 8. For demonstration purposes, we assume a solution to surface elevation of the form

$$\zeta(x,t) = a\cos(\omega t - kx). \tag{12}$$

Equation (12) is strictly applicable for a prismatic channel, but we use it here to simplify trigonometric expansion. Inserting (12) into (4), for small kL (4) can be approximated at x = 0 as

$$U(x=0,t) = -\frac{L\omega a}{H}\sin(\omega t) - \frac{a}{H}\frac{\omega}{k} \cdot [2\sin(-kL/2)\sin(\omega t - kL/2) + kL\sin(\omega t - kL)]. \tag{13}$$

The first term on the right-hand side of (13) is from the rigid lid part of (4), and the second term (in brackets) contains sine terms with phase lagged relative to the local depth $H = a\cos(\omega t) + h$ by $O(k\Delta x)$; this second term represents the lagged surface gradient along the tidal system and is shown separately in Figure 8, along with the local depth and the resultant velocity. Increasing the surface phase lag (larger k) and/or decreasing depth both generate more negative velocity skew (Figure 8); the depth for an equivalent pressure gradient is smaller on ebb than flood as the lagged surface gradient shifts the timing of slack water later in the tidal cycle. With a small phase lag held constant, changes to depth can only affect the magnitude of the skew, with more negative skew for shallower depths (Figure 8b). Of course, the situation in Skagit Bay is more complex than presented in

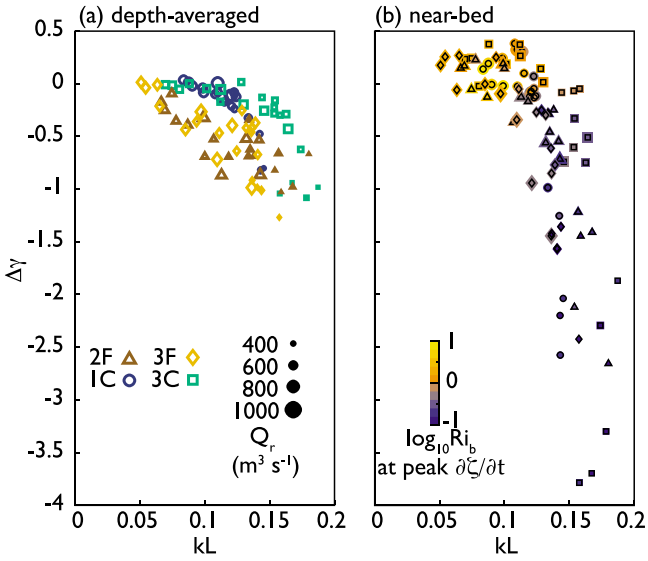

Figure 7. Difference between daily velocity skewness and tidal asymmetry, as a function of the deviation from a rigid lid (equation (10)). Size of symbol denotes magnitude of daily mean river discharge. Color shading in Figure 7b indicates Ri_b at time of peak falling water.

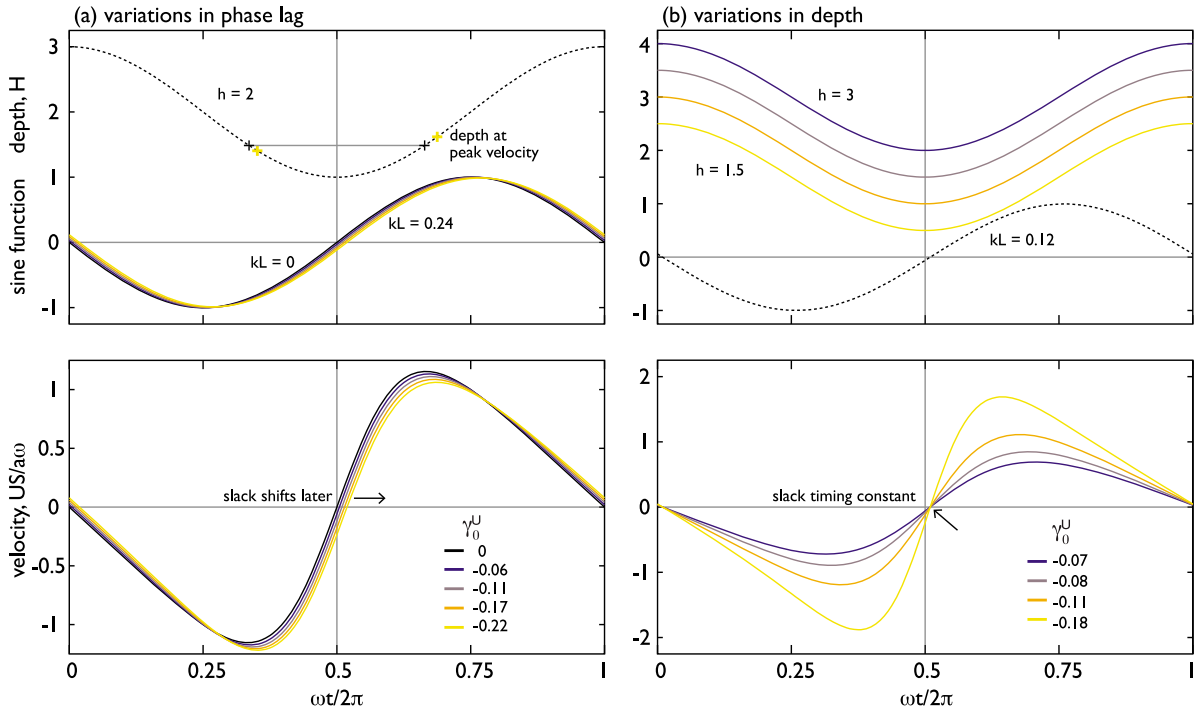

Figure 8. These simple examples, evaluated numerically using equation (13), show that ebb-dominant velocity skew is generated when the phase of the pressure gradient, integrated landward to the shoreline, lags that of the local depth. (a) Increasing the magnitude of the phase lag shifts slack water later in the tidal cycle and skews the velocity distribution toward ebb dominance. Additionally, the timing of peak ebb and flood is shifted asymmetrically about low water for increasing phase lag; the crosses show the time of peak velocity for $kL = 0$ and $kL = 0.04$ in black and red, respectively. (b) Changing the local depth relative to the tidal amplitude increases the severity of the skew but does not affect the timing of slack.

these examples, but the general mechanism appears to be relevant.

[50] The interaction between the phase lag and local depth in our observations is shown in a series of stage velocity diagrams (Figure 9), where the elevation of peak flood and ebb are shifted higher and lower, respectively, relative to midtide. There is a velocity deficit (relative to the velocity predicted for a linearized, rigid lid (equation (5)) on flood prior to midtide and a velocity enhancement on ebb following midtide, such that peak ebb and peak flood velocities occur at different depths, as illustrated in Figure 8a. On the flat, the drag coefficient was larger on flood than ebb (not shown), presumably due to the presence of vegetation upcurrent on flood (Figure 1b). *Lacy and Wyllie-Echeverria* [2011] reported C_d 4 to 10 times larger over patches of *Zostera* than over bare sand; our observations indicated an increase of at least a factor of 2. Increased drag shifts peak flood velocity to later in the flood when the water column is deeper, effectively reducing peak stress on flood.

[51] Our observations on the tidal flat ran counter to our initial assumption that the shallow, shoaling tidal flat would lead to flood-dominant velocities [e.g., *Speer and Aubrey*, 1985; *Friedrichs and Aubrey*, 1988; *Friedrichs and Madsen*, 1992]. It was reasonable to anticipate that the distributary channels might be ebb dominant due to the river discharge; the similar response of the flats, however, was surprising. *Friedrichs et al.* [1992] showed that ebb-dominant forcing at the tidal boundary can generate flood-dominant currents farther into the tidal system as the tidal wave distortion takes a finite distance to evolve. To understand our observations in the context of the phase lags that we observed, we calculated skewness (Figure 8) for a tidal propagation model containing an overtide term that increases in magnitude with distance into the estuary [*Friedrichs and Aubrey*, 1994]:

$$\zeta(x,t) = a\cos(\omega t - kx) - \frac{a\gamma kx}{2}\cos(2\omega t - 2kx - \pi/2). \quad (14)$$

The parameter γ is a morphological asymmetry factor that accounts for tidal variations in depth and width [*Friedrichs and Madsen*, 1992]. The water level from (14) is inserted into (4) to solve for velocity, though again the solution does not apply directly to tidal flats, which are more appropriately represented with Bessel functions that decay with distance [e.g., *Prandle and Rahman*, 1980; *Prandle*, 2009]. The simple formulation of γ in conjunction with an overtide that contributes to a principal harmonic is sufficient to demonstrate how velocity skewness responds to duration asymmetry.

[52] As the frictional scale relative to the length of the tidal system, kL, increases along the vertical axis of each plot in Figure 10, the magnitude of the surface distortion increases. For $\gamma > 0$ (top row in Figure 10), duration asymmetry becomes shorter rising, as predicted for a shoaling estuary [*Friedrichs and Aubrey*, 1988]. In contrast to the velocity skew that would be predicted by a rigid lid approximation (equation (5)), velocity skew is initially ebb dominant at the seaward end of the flat, due to the effect of the lagged

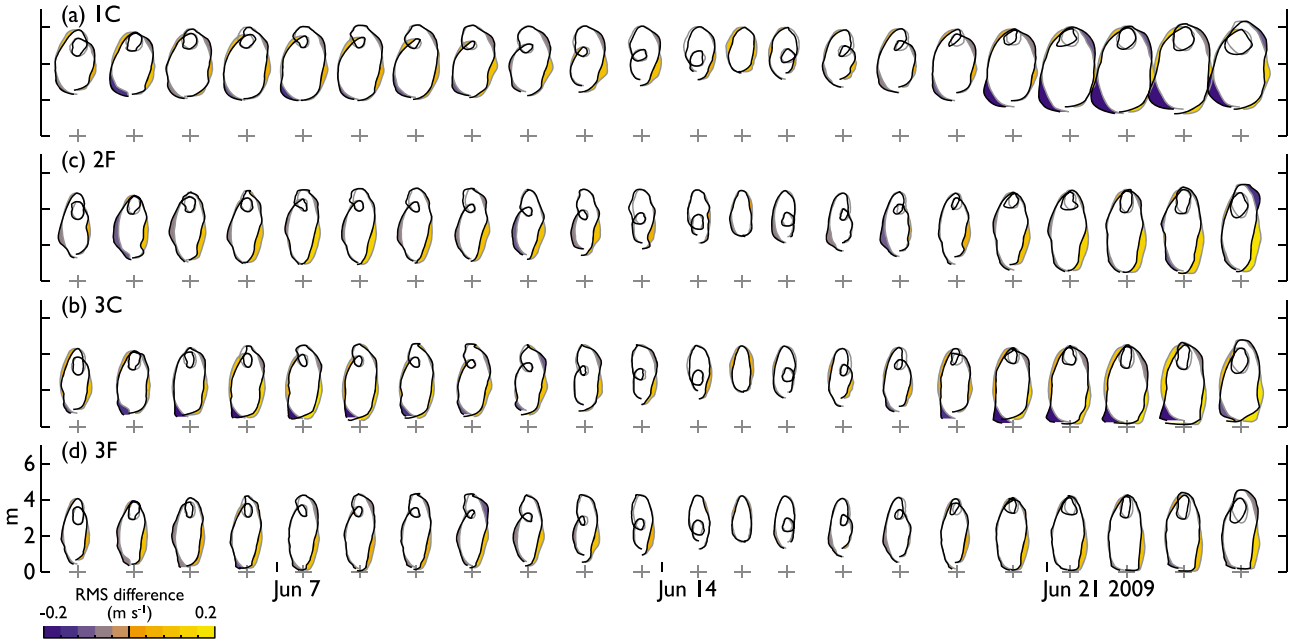

Figure 9. Stage velocity diagrams, offset by day: observed velocity and depth (black lines) and predicted velocity for a rigid lid (equation (6)) using water level observations at Seattle as an offshore tidal elevation (gray lines). Observed depth is shown with the predicted velocity. The discrepancies between the two curves are shaded: weaker velocities relative to U_0 are shaded yellow, and stronger velocities are shaded blue. The intensity of the shading is varied according to the RMS velocity difference for each flood and ebb period.

pressure gradient relative to local depth, as we observed above. With increasing landward distance the velocity skew becomes flood dominant, as described by *Friedrichs et al.* [1992]. The middle row in Figure 10 shows the solution with no overtide contribution; in the absence of any duration asymmetry, the effect of a phase lag on velocity skew is evident. For $\gamma < 0$ (bottom row in Figure 10), distortion leads to shorter-falling tides with distance into the estuary [*Speer and Aubrey*, 1985] and the velocity skew is also ebb dominant. In all cases, the difference between velocity skew and duration asymmetry is negative; the local phase lag provides a source of negative velocity skew that is only overcome by significant distortion with distance into the estuary or across the tidal flat such that a portion of the lower estuary may be ebb dominant while the upper reaches are flood dominant.

4.3. Competing Effects of Fluvial Discharge

[53] In the absence of freshwater discharge, fortnightly changes in duration asymmetry and velocity skew that occur in Skagit Bay can be reasonably predicted based on tidal harmonics. The effects of fluvial discharge are less predictable, in part because of the inherent variability in river flows, but also because the river discharge may contribute both ebb- and flood-dominant velocity skew. We include a brief summary of our observations here, while a more thorough discussion of baroclinicity and the effects on sediment transport at this site can be found in the work of *Ralston et al.* [2012].

[54] The imposition of a mean river flux negatively shifts velocity skew. This is illustrated in Figure 11, where we add a range of river fluxes to the tidal solution of (13). The river flux shifts the timing of slack before flood later in the tidal cycle, similar to the case where tidal discharge is delayed relative to the local depth phase. In contrast to the effect of a frictionally generated lag in tidal discharge, however, slack before ebb is shifted earlier. This effect of the river flux on the timing of slack before ebb is not apparent in our observations from Skagit Bay because at high tide the effective river velocity is small. The alongshore width of the freshwater discharge is 5 to 10 times greater at high tide than at low tide, when the discharge is constrained to the distributary channel network.

[55] The importance of channelized river flux in generating negative velocity skew depends on the across-shore position. For locations within the distributary channels and landward of the low-water shoreline (wetted front), the continued volume flux after the flats have drained reinforces ebb skew. This same volume flux has a more limited effect at the lip of the flats where the flow is deeper. Consequently, the river flux contributes greater ebb skew with landward distance, as the fraction of time that the flats are exposed during the tidal cycle increases [*Ralston et al.*, 2012]. Within Skagit Bay, this effect modulates with the spring-neap cycle owing to the fortnightly variation in LLW, and is evident in our observations at 3C during spring tides (Figure 9c). Note that this channelized discharge is separate from the delayed tidal discharge at 1C (the timing of this is particularly evident in Figure 3c).

[56] Although the river discharge will contribute negative velocity skew in a depth-averaged sense, stratification shifts near-bed velocity skew positive. Relative to duration asymmetry, near-bed velocity skew was flood dominant when Ri_b exceeded 1 throughout the time of peak ebb (Figure 7b)

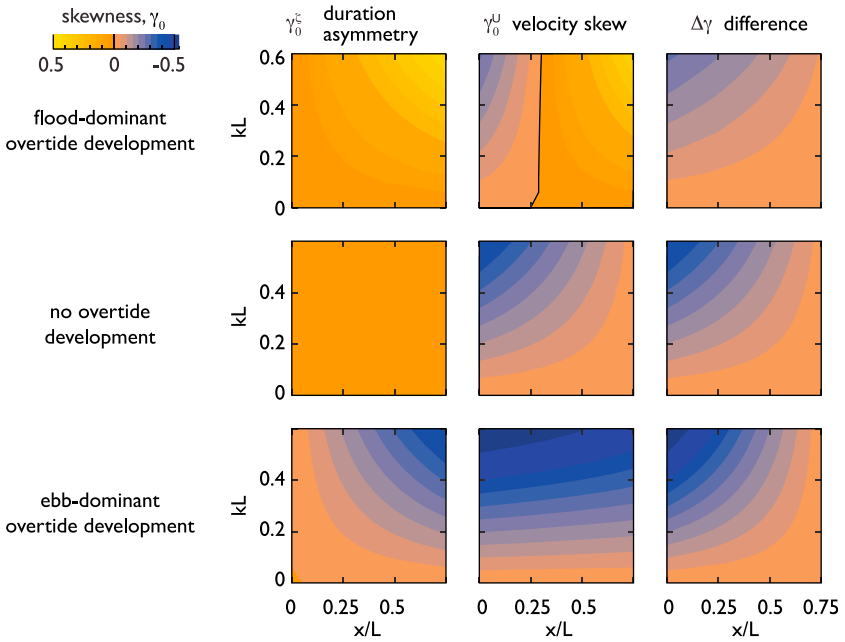

Figure 10. Skewness as a function of position within estuary (x/L) and phase lag (kL), based on evaluation of the simplified solution using (14). Shown are (left) duration asymmetry, (middle) velocity skew, and (right) the difference between velocity skew and duration asymmetry. The middle row shows the case for no overtide development within the estuary. The top row shows the case for the growth of shorter-rising asymmetry ($\gamma = 0.5$), and the bottom row shows the case for shorter-falling asymmetry ($\gamma = -0.5$).

and near-bed velocity skew (Figure 4f) became more flood dominant with increased discharge.

[57] Two factors contribute to this asymmetry/skew pattern. First, the baroclinic pressure gradient provides a landward directed acceleration in the near-bed region (Figure 3). Second, stratification on ebb limits bottom stress relative to flood. There was a systematic reduction in near-bed velocities on ebb for $Ri_b > 1$ (Figure 12), indicative of tidal straining [*Simpson et al.*, 1990]. In contrast, the flood tides were less stably stratified. The tendency for the ebbs to stratify via straining of the horizontal salinity field leads to near-bed flood dominance [*Jay*, 1991]. For the largest spring tides, this effect was negated when stratification was mixed out through peak ebb.

[58] *Ralston et al.* [2012] considered how sediment transport was affected by this competition between the ebb-directed fluvial discharge and flood-dominant bottom stresses caused by estuarine processes. They found that the baroclinicity enhanced trapping of sediment delivered by the river on the tidal flats during neap tides, and that sediment trapping also depends on settling-and-scour lag, particularly for finer particles. The high velocities and stresses in the distributary channels during low tides moved sediment off of the tidal flats such that sediment export occurred predominantly during spring low tides that exposed a greater portion of the flats.

5. Conclusions and Discussion

[59] We have presented an overview of velocity skew derived from incident asymmetry, frictionally generated phase lags, fluvial discharge, and baroclinicity to explain observations from the tidal flats and distributary channels of the macrotidal Skagit River delta. The incident asymmetry that modulates with the spring-neap cycle was evident as alternating flood- and ebb-dominant velocity skew, largely

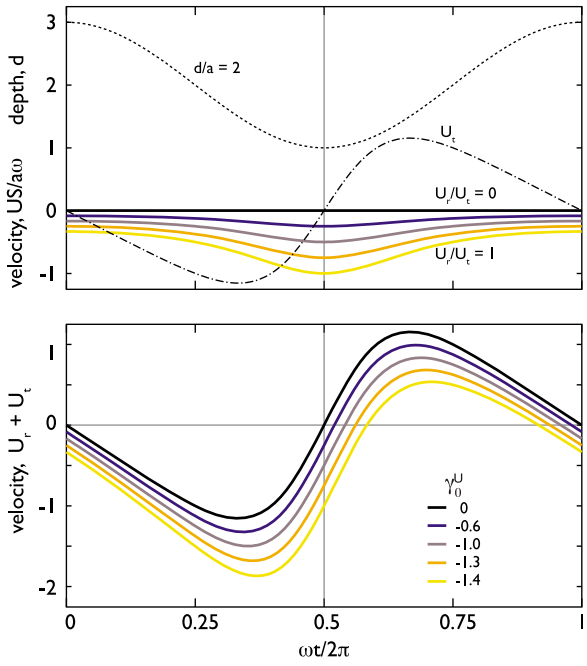

Figure 11. This simple example shows that the superposition of a mean river discharge on tidal flow results in ebb-directed velocity skew. The skewnesses of U_t and U_r alone are 0 and -1.2, respectively. The effect of the river discharge is assumed to not affect the tidally variable depth.

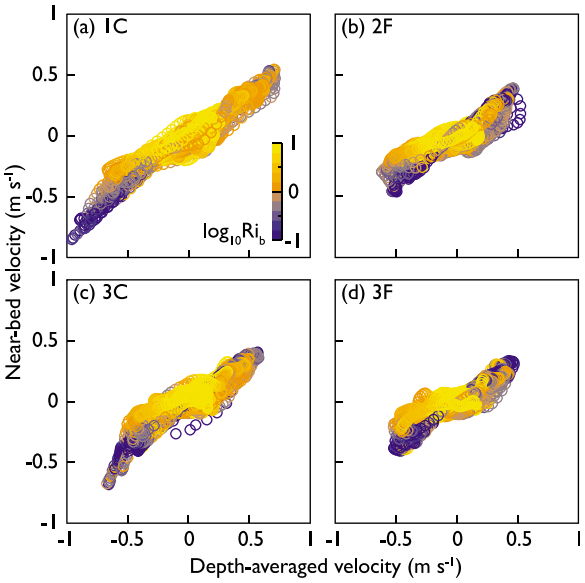

Figure 12. Near-bed velocity as function of depth-averaged velocity, shaded according to Ri_b: stations (a) 1C, (b) 2F, (c) 3C, and (d) 3F.

due to the near-quadrature relationship between velocity and elevation. We observed that three factors contributed to local asymmetries and a deviation from what would be expected based on a rigid lid: (1) phase lags between the surface gradient and local depth lead to ebb dominance, (2) fluvial discharge contributes to ebb dominance at low tide, and (3) baroclinicity leads to near-bed flood dominance even in a shallow, macrotidal system.

[60] Based on a scaling of the continuity equation, the use of a rigid lid approximation for translating duration asymmetry to velocity skew in a short, shallow tidal embayment loses validity as (1) tidal amplitude increases, depth decreases, and/or drag increases; (2) embayment length increases; and (3) width of embayment increases landward. On tidal flats, decreasing bed slope contributes to this loss of validity, as smaller slopes lead to greater tidal excursions as a function of a given tidal amplitude. These factors lead to frictionally generated phase lags in the surface pressure gradient and result in negative velocity skew. Consequently, larger spring tides tend to have greater ebb dominance. Spring tides also exposed a greater fraction of the tidal flats at LLW, altering the proportion of the delta and flats that are affected by an ebb-directed fluvial discharge. The baroclinic contribution from the river flow resulted in a flood-dominant near-bed velocity skew, countering the ebb-directed mechanisms particularly around neap tides and on the flats away from the distributary channel network. Our observations are notable in the context of previous studies of tidal asymmetry [e.g., *Speer and Aubrey*, 1985; *Friedrichs and Aubrey*, 1988; *Friedrichs et al.*, 1992] as our analyses indicate that these previously described mechanisms are relevant over very short spatial scales of just a few kilometers.

[61] Central to these observations are two variables: the fortnightly modulation in tidal range and event-scale changes in river discharge. In drawing conclusions about the cumulative effects of these mechanisms for long-term geomorphic evolution, it is important to place these comparatively brief observations in the context of the annual discharge and semiannual tidal modulation (Figure 13). On an annual basis, the magnitude of the duration asymmetry is maximum and minimum at the vernal solstices and equinox, respectively. The mean duration asymmetry at Seattle for 2009 was 0.02; this implies that asymmetry in the tide alone may be relatively unimportant to sediment transport in Puget Sound at very long time scales, despite significant fortnightly modulations.

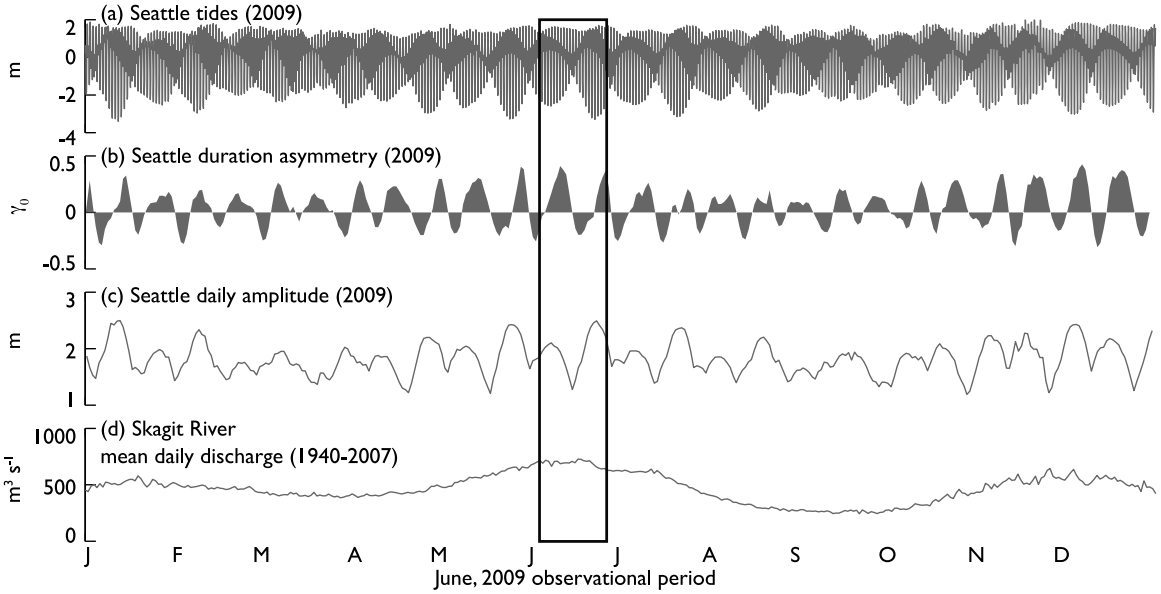

Figure 13. (a) Water level at Seattle NOS station 9447130 for 2009. (b) Lunar day duration asymmetry at Seattle. (c) Daily greater diurnal tidal amplitude. (d) Daily mean discharge for the Skagit River at Mount Vernon for 1940–2007. The time period for observations presented in this paper is outlined.

Table A1. Harmonic Amplitudes and Phases Obtained From Different Record Lengths[a]

	Reported		53 Day Records				19 Day Records							
			Seattle		1C		Seattle		1C		3C		3F	
Q1	8	250°	10	254°	10	254°	-	-	-	-	-	-	-	-
			4.6	31°	5.3	29°	-	-	-	-	-	-	-	-
O1	46	255°	48	258°	48	259°	43	252°	43	254°	42	255°	43	254°
			4.9	6°	4.9	5°	5.7	8°	6.0	7°	6.1	7°	5.6	8°
K1	83	277°	101	281°	101	282°	104	272°	104	274°	104	275°	105	274°
			4.8	3°	5.1	3°	5.4	4°	5.7	3°	6.6	4°	6.8	3°
MU2	3	237°	6	262°	6	263°	-	-	-	-	-	-	-	-
			1.6	14°	1.6	18°	-	-	-	-	-	-	-	-
N°	22	341°	25	344°	26	346°	-	-	-	-	-	-	-	-
			1.5	3°	1.8	4°	-	-	-	-	-	-	-	-
M2	107	11°	109	10°	112	12°	100	10°	101	13°	102	14°	102	13°
			1.5	1°	1.6	1°	10.1	5°	9.8	6°	10.1	6°	10.8	5°
L2	4	56°	4	45°	4	47°	-	-	-	-	-	-	-	-
			1.2	17°	1.3	23°	-	-	-	-	-	-	-	-
S2	27	37°	19	50°	18	53°	18	46°	17	49°	17	53°	18	53°
			1.6	4°	1.7	5°	9.3	30°	9.0	30°	9.3	30°	9.5	35°
MK3	3	78°	5	86°	5	74°	-	-	-	-	-	-	-	-
			0.8	9°	0.9	12°	-	-	-	-	-	-	-	-
M4	2	200°	2	194°	1	124°	2	190°	2	115°	1	110°	*	*
			0.3	9°	0.4	22°	0.3	12°	0.3	9°	0.5	45°	*	*
S4	0	0°	1	147°	*	*	0	149°	0	203°	*	*	*	*
			0.3	34°	*	*	0.3	38°	0.2	31°	*	*	*	*
M6	1	314°	1	312°	1	353°	1	299°	1	340°	*	*	*	*
			0.3	23°	0.4	21°	0.5	41°	0.5	43°	*	*	*	*

[a]Only constituents with a signal-to-noise ratio >2 are reported. For each constituent, the first row reports the amplitude in cm and phase in degrees relative to GMT, and the second row reports the 95% confidence intervals. All results obtained with T-TIDE [*Pawlowicz et al.*, 2002].

[62] The spring-neap modulation of asymmetry, however, may be important to the short-term fate of sediment deposited on the flat by episodic events. For example, sediment export from the lower flats may only occur at specific times of the year when tidal conditions are right. In this manner, the timing and delivery of sediment to the flats due to the annual cycle of river discharge may affect the importance of the incident principal tide asymmetry. Our observations coincided with both the spring snowmelt freshet and perigean solstice tides. Consequently, conclusions regarding both the ebb dominance of depth-averaged currents and the flood-directed near-bed skew could overestimate the magnitude of these effects compared to, for example, a 3 week period in late summer when discharge is reduced, tidal ranges are smaller, and the magnitude of fortnightly modulation in incident duration asymmetry is reduced. Our observations highlight the short-term variability in processes that contribute to sediment transport, and the effects of the full range of this variance should be considered in studies where tides and river flows are important contributors to long-term geomorphic evolution.

Appendix A

[63] Least squares harmonic analysis of tidal elevation and velocity was performed using MATLAB and the toolbox T-TIDE [*Pawlowicz et al.*, 2002]. To minimize errors produced by harmonic analysis of a severely truncated tidal record (where the sensor goes dry or has an extended period of quasi-stationary water level), we analyzed a short 19 day record (6–21 June) with no extreme lower-low tides. For comparison, we also analyzed longer 53 day records at Seattle and 1C (Tables A1 and A2); the longer record

Table A2. Ellipse Parameters for Selected Harmonics

Component	O1	K1	M2	S2	M4
Semimajor axis (m s^{-1})					
1C	0.08	0.19	0.35	0.08	0.02
2F	0.05	0.13	0.25	0.05	0.02
3C	0.06	0.13	0.26	0.07	0.01
3F	0.04	0.12	0.23	0.05	0.01
Phase (deg GMT)					
1C	168.3	187.4	291.9	323.2	318.3
2F	181.3	189.9	286.8	335.2	40.6
3C	184.7	192.9	290.2	334.2	159.6
3F	175.1	187.6	285.4	335.9	18.7
Eccentricity					
1C	0.18	0.17	0.17	0.07	−0.68
2F	0.09	0.20	0.24	0.06	0.15
3C	−0.10	0.14	0.15	−0.08	−0.12
3F	−0.12	0.16	0.17	−0.14	0.39
Inclination (deg)					
1C	34.8	30.6	28.0	24.9	129.5
2F	29.0	18.4	16.0	6.8	34.9
3C	17.2	13.6	14.3	9.4	22.1
3F	26.0	18.5	19.7	13.4	12.4

Table A3. Asymmetry Metrics Derived From Harmonic Analysis

	Elevation			Velocity[a]		
	1C	3C	3F	1C	3C	3F
M4/M2	0.02	0.01	0.00	0.04	0.05	0.06
2 M2–M4	270°	279°	277°	160°	63°	187°
D2/D1	0.70	0.70	0.69	1.33	1.35	1.42
2D1–D2	155°	155°	155°	62°	88°	79°

[a]Velocity results are for depth-averaged across-shore velocity.

resolves some of the neighboring constituents missed with the shorter time series. The semimajor axes of the M_2 and K_1 depth-averaged velocity ellipses were aligned across-shore (Figure 1b), with positive, low eccentricity indicating predominantly rectilinear currents with counterclockwise rotation. The phase differences between the current ellipses and water elevation were 80°–85° (Table A3).

[64] In the context of asymmetry metrics that rely on harmonic analysis, there appeared to be a decrease in nonlinearity with landward distance (Table A2) as the incident M_4 transitioned to an internally generated M_4. The M_4 velocity ellipse at 1C was aligned along isobaths (Figure 1b), parallel to the deep channel at the seaward edge of the flats, while M_4 ellipses farther landward were oriented perpendicular to isobaths, indicating a rectification of currents over a short distance. Simple phase differences, summarized in Table A2, indicated a mix of ebb-dominant and flood-dominant conditions between elevation and velocity, and principal tides and overtides. These results highlight the difficulty in reconciling the observed asymmetry using harmonic constituents alone.

[65] **Acknowledgments.** Discussions with Rocky Geyer and Britt Raubenheimer were particularly helpful. Peter Traykovski and Rocky Geyer contributed to the field design, and Jay Sisson helped with the deployment. We thank Carl Friedrichs and an anonymous reviewer for providing detailed reviews that improved the manuscript. N.J.N. was supported by USGS/WHOI Postdoctoral Scholar funds. This work was supported by the Office of Naval Research.

References

Ahnert, F. (1960), Estuarine meanders in the Chesapeake Bay area, *Geogr. Rev.*, *50*, 390–401.

Bagnold, R. (1966), An approach to the sediment transport problem from general physics, *U.S. Geol. Surv. Prof. Pap.*, *422-I*, 42 pp.

Blanton, J. O., G. Q. Lin, and S. A. Elston (2002), Tidal current asymmetry in shallow estuaries and tidal creeks, *Cont. Shelf Res.*, *22*, 1731–1743.

Boon, J. D., and R. J. Byrne (1981), On basin hypsometry and the morphodynamic response of coastal inlet systems, *Mar. Geol.*, *40*, 27–48.

Dronkers, J. (1986), Tidal asymmetry and estuarine morphology, *Neth. J. Sea Res.*, *20*, 117–131.

Elgar, S., and R. T. Guza (1985), Observations of bispectra of shoaling surface gravity waves, *J. Fluid Mech.*, *161*, 425–448.

Emery, W. J., and R. E. Thomson (2001), *Data Analysis Methods in Physical Oceanography*, 2nd ed., 654 pp., Elsevier, Amsterdam.

Fagherazzi, S., P. Wiberg, and A. Howard (2003), Tidal flow field in a small basin, *J. Geophys. Res.*, *108*(C3), 3071, doi:10.1029/2002JC001340.

Fortunato, A. B., and A. Oliveira (2005), Influence of intertidal flats on tidal asymmetry, *J. Coastal Res.*, *21*, 1062–1067.

French, J., and D. Stoddart (1992), Hydrodynamics of salt marsh creek systems: Implications for marsh morphological development and material exchange, *Earth Surf. Processes Landforms*, *17*, 235–252.

Friedrichs, C. T. (2010), Barotropic tides in channelized estuaries, in *Contemporary Issues in Estuarine Physics*, edited by A. Valle-Levinson, pp. 27–61, Cambridge Univ. Press, Cambridge, U. K.

Friedrichs, C. T. (2012), Tidal flat morphodynamics: A synthesis, in *Treatise on Estuarine and Coastal Science*, vol. 3, *Estuarine and Coastal Geology and Geomorphology*, edited by J. D. Hansom and B. W. Flemming, Academic, Waltham, Mass., in press.

Friedrichs, C. T., and D. G. Aubrey (1988), Non-linear tidal distortion in shallow well-mixed estuaries: A synthesis, *Estuarine Coastal Shelf Sci.*, *27*, 521–545.

Friedrichs, C. T., and D. G. Aubrey (1994), Tidal propagation in strongly convergent channels, *J. Geophys. Res.*, *99*, 3321–3336.

Friedrichs, C. T., and D. G. Aubrey (1996), Uniform bottom shear stress and equilibrium hypsometry of intertidal flats, in *Mixing in Estuaries and Coastal Seas*, *Coastal Estuarine Stud.*, vol. 50, edited by C. Pattiaratchi, pp. 404–429, AGU, Washington, D. C.

Friedrichs, C. T., and O. S. Madsen (1992), Nonlinear diffusion of the tidal signal in frictionally dominated embayments, *J. Geophys. Res.*, *97*, 5637–5650.

Friedrichs, C. T., D. R. Lynch, and D. G. Aubrey (1992), Velocity asymmetries in frictionally dominated tidal embayments: Longitudinal and lateral variability, in *Dynamics and Exchanges in Estuaries and the Coastal Zone*, *Coastal Estuarine Stud.*, vol. 40, edited by D. Prandle, pp. 276–312, AGU, Washington, D. C.

Geyer, W. R. (1993), Three-dimensional tidal flow around headlands, *J. Geophys. Res.*, *98*, 955–966.

Godin, G. (1991), The analysis of tides and currents, in *Tidal Hydrodynamics*, edited by B. B. Parker, pp. 675–709, John Wiley, New York.

Heath, R. (1980), Phase relations between the over- and fundamental-tides, *Ocean Dyn.*, *33*, 177–191, doi:10.1007/BF02226319.

Hoitink, A. J. F., P. Hoekstra, and D. S. van Maren (2003), Flow asymmetry associated with astronomical tides: Implications for the residual transport of sediment, *J. Geophys. Res.*, *108*(C10), 3315, doi:10.1029/2002JC001539.

Huntley, D. (1988), A modified inertial dissipation method for estimating seabed stresses at low Reynolds numbers, with application to wave/current boundary layer measurements, *J. Phys. Oceanogr.*, *18*, 339–346.

Jay, D. A. (1991), Internal asymmetry and anharmonicity in estuarine flows, in *Tidal Hydrodynamics*, edited by B. B. Parker, pp. 521–543, John Wiley, New York.

Kirby, R. (2000), Practical implications of tidal flat shape, *Cont. Shelf Res.*, *20*, 1061–1077.

Lacy, J. R., and S. Wyllie-Echeverria (2011), The influence of current speed and vegetation density on flow structure in two macrotidal eelgrass canopies, *Limnol. Oceanogr. Fluids Environ.*, *1*, 38–55, doi:10.1215/21573698-1152489.

LeBlond, P. H. (1978), On tidal propagation in shallow rivers, *J. Geophys. Res.*, *83*, 4717–4721.

Lincoln, J., and D. Fitzgerald (1988), Tidal distortions and flood dominance at five small tidal inlets in southern Maine, *Mar. Geol.*, *82*, 133–148.

McBride, A., K. Wolf, and E. Beamer (2006), Skagit Bay nearshore habitat mapping, technical report, Skagit River Syst. Coop., La Conner, Wash.

Nidzieko, N. J. (2010), Tidal asymmetry in estuaries with mixed semidiurnal/diurnal tides, *J. Geophys. Res.*, *115*, C08006, doi:10.1029/2009JC005864.

Nidzieko, N. J., J. L. Hench, and S. G. Monismith (2009), Lateral circulation in well-mixed and stratified estuarine flows with curvature, *J. Phys. Oceanogr.*, *39*, 831–851, doi:10.1175/2008JPO4017.1.

Parker, B. B. (1991), The relative importance of the various nonlinear mechanisms in a wide range of tidal interactions, in *Tidal Hydrodynamics*, edited by B. B. Parker, pp. 237–268, John Wiley, New York.

Pawlowicz, R., B. Beardsley, and S. Lentz (2002), Classical tidal harmonic analysis including error estimates in MATLAB using T-TIDE, *Comput. Geosci.*, *28*, 929–937.

Postma, H. (1961), Transport and accumulation of suspended matter in the Dutch Wadden Sea, *Neth. J. Sea Res.*, *1*, 148–180.

Prandle, D. (2009), *Estuaries: Dynamics, Mixing, Sedimentation and Morphology*, 248 pp., Cambridge Univ. Press, Cambridge, U. K.

Prandle, D., and M. Rahman (1980), Tidal response in estuaries, *J. Phys. Oceanogr.*, *10*, 1552–1573.

Pritchard, D. (2005), Suspended sediment transport along an idealised tidal embayment: Settling lag, residual transport and the interpretation of tidal signals, *Ocean Dyn.*, *55*, 124–136, doi:10.1007/s10236-005-0004-7.

Pritchard, D., and A. J. Hogg (2003), Cross-shore sediment transport and the equilibrium morphology of mudflats under tidal currents, *J. Geophys. Res.*, *108*(C10), 3313, doi:10.1029/2002JC001570.

Ralston, D. K., and M. T. Stacey (2007), Tidal and meteorological forcing of sediment transport in tributary mudflat channels, *Cont. Shelf Res.*, *27*, 1510–1527, doi:10.1016/j.csr.2007.01.010.

Ralston, D. K., W. R. Geyer, P. A. Traykovski, and N. J. Nidzieko (2012), Effects of estuarine and fluvial processes on sediment transport over deltaic tidal flats, *Cont. Shelf Res.*, doi:10.1016/j.csr.2012.02.004, in press.

Scully, M., and C. Friedrichs (2003), The influence of asymmetries in overlying stratification on near-bed turbulence and sediment suspension in a partially mixed estuary, *Ocean Dyn.*, *53*, 208–219.

Seim, H. E., J. O. Blanton, and S. Elston (2006), Tidal circulation and energy dissipation in a shallow, sinuous estuary, *Ocean Dyn.*, *56*, 360–375, doi:10.1007/s10236-006-0078-x.

Simpson, J. H., J. Brown, J. Matthews, and G. Allen (1990), Tidal straining, density currents, and stirring in the control of estuarine stratification, *Estuaries*, *13*, 125–132.

Speer, P. E., and D. G. Aubrey (1985), A study of non-linear tidal propagation in shallow inlet/estuarine systems. Part II: Theory, *Estuarine Coastal Shelf Sci.*, *21*, 207–224.

Speer, P. E., D. G. Aubrey, and C. T. Friedrichs (1991), Nonlinear hydrodynamics of shallow tidal inlet/bay systems, in *Tidal Hydrodynamics*, edited by B. B. Parker, pp. 321–339, John Wiley, New York.

Van Straaten, L., and P. Kuenen (1958), Tidal action as a cause of clay accumulation, *J. Sediment. Petrol.*, *28*, 406–413.

van Veen, J., A. J. F. van der Spek, M. J. F. Stive, and T. Zitman (2005), Ebb and flood channel systems in the Netherlands tidal waters, *J. Coastal Res.*, *21*, 1107–1120, doi:10.2112/04-0394.1.

N. J. Nidzieko, Horn Point Laboratory, University of Maryland Center for Environmental Science, 2020 Horns Point Rd., Cambridge, MD 21613, USA. (nidzieko@umces.edu)

D. K. Ralston, Applied Ocean Physics and Engineering, Woods Hole Oceanographic Institution, 266 Woods Hole Rd., Woods Hole, MA 02540, USA. (dralston@whoi.edu)